Complete Measurement of $S(^1D_2)$ Photofragment Alignment from Abel-Invertible Ion Images

T. Peter Rakitzis,[1,3,*] Peter C. Samartzis,[2,3] and Theofanis N. Kitsopoulos[2,3]

[1]*Department of Physics, University of Crete, P.O. 2208, 71003 Voutes-Heraklion, Greece*

[2]*Department of Chemistry, University of Crete, Leof. Knosou, 71409 Heraklion, Greece*

[3]*Institute of Electronic Structure and Laser, Foundation for Research and Technology-Hellas, 711 10 Heraklion-Crete, Greece*

(Received 16 January 2001; published 29 August 2001)

A novel method to measure directly the photofragment alignment from Abel-invertible two-dimensional ion images, as a function of photofragment recoil velocity, is demonstrated for $S(^1D_2)$ atoms from the photodissociation of carbonyl sulfide at 223 nm. The results are analyzed in terms of coherent and incoherent contributions from two dissociative states, showing that the phase differences of the asymptotic wave functions of the fast and slow recoil-velocity channel are approximately $\pi/2$ and 0, respectively.

DOI: 10.1103/PhysRevLett.87.123001 PACS numbers: 33.80.Gj, 34.20.Gj, 34.20.Mq, 34.50.Lf

A theoretical formalism has been presented describing the complete photofragment polarization in terms of coherent and incoherent contributions from multiple dissociative states of different symmetry [1]. Using a similar formalism [2], the complete photofragment alignment and orientation have been measured for the $Cl(^2P_J)$ photofragments from the photodissociation of Cl_2 and ICl [3,4]. In both cases, the *coherent* contribution to the photofragment alignment and orientation have been shown to oscillate as a function of the dissociation energy [4–6]. These oscillations give a direct measure of the energy-dependent phase difference of the asymptotic wave functions associated with the two interfering dissociative states, providing a new and accurate spectroscopy of potential energy surfaces in molecular photodissociation. In the case of Cl_2, the *incoherent* contributions to the photofragment alignment were shown to be sensitive to long-range nonadiabatic processes [3,7,8].

Although these photofragment polarization measurements have provided unprecedented detail and insight into the photodissociation process, they were performed on diatomic molecules which photodissociate into monoenergetic fragments. Photodissociation of polyatomic molecules yields, in general, photofragments with broad translational distributions, so that both the photofragment velocity and the angular distribution must be measured simultaneously.

Two-dimensional (2D) ion imaging [9], especially in its refined form called velocity mapping [10], has become an important and widely used technique in photofragment and photoelectron spectroscopy. The important strength of this 2D technique is that the full three-dimensional (3D) velocity-dependent angular distribution can be inverted from the 2D image using the inverse-Abel transform, from images that possess cylindrical symmetry parallel to the image plane. For pump-probe experiments, such cylindrical symmetry is achieved, in general, when both pump and probe laser polarizations are parallel to each other and the imaging plane. However, a single image does not suffice to measure the complete photofragment alignment. Until recently, attempts to measure photofragment alignment using 2D imaging have used several noncylindrically symmetric images that have been analyzed with forward-convolution methods.

In this Letter, we demonstrate for the first time the *direct,* simultaneous measurement of the recoil velocity and complete alignment of the $S(^1D_2)$ photofragments from the photodissociation of carbonyl sulfide (OCS) from unnormalized Abel-invertible (2D) velocity images, using various combinations of linearly and circularly polarized light, and different $(2 + 1)$ resonance enhanced multiphoton ionization (REMPI) transitions.

A 5% mixture of OCS in He is expanded supersonically parallel to the electric field of a time-of-flight mass spectrometer via a piezoelectrically actuated pulsed-molecular beam. The skimmed molecular beam is intersected perpendicularly by focused photolysis (223 nm) and probe laser beams (using $f = 300$ and 200 mm spherical lenses, respectively). The laser propagation directions are chosen either parallel or perpendicular to each other, to allow the laser polarizations to be parallel to each other and the imaging plane. The probe beam is the frequency-doubled output of an Excimer-pumped dye laser (Lumonics HyperEX400, ELTO 1233), and the photolysis laser is the output of a YAG-pumped MOPO (730D10 Spectra Physics). The $S(^1D_2)$ photofragments are ionized by $(2 + 1)$ REMPI via the $^1P_1$ or $^1F_3$ states at 291.48 and 288.19 nm, respectively [11]. Ions produced are velocity mapped onto a position-sensitive imaging detector. The imaging detector gain is pulsed at the appropriate time to detect only $^{32}S^+$ ions.

Six 2D ion images of the $S(^1D_2)$ atoms are shown in Fig. 1. Each image represents a 2D projection of the 3D photofragment-velocity distribution. Two distinct rings of $S(^1D_2)$ atoms are visible, caused by a bimodal CO $(v = 0)$ rotational distribution: The outer (fast) component of $S(^1D_2)$ atoms is correlated with CO molecules with a narrow rotational distribution peaked at $J \approx 55$, whereas the inner (slow) component is correlated with CO molecules with a narrow rotational distribution peaked at $J \approx 65$ [12,13].

The angular distribution $I(\theta)$ of photofragments from achiral molecules and a cylindrically symmetric multiphoton process can be described by an expansion of even Legendre polynomials. For a one-photon photodissociation (in the dipole approximation) and two-photon resonant detection (as is 2 + 1 REMPI), the expansion is terminated by the 6th order Legendre polynomial:

$$I(\theta) = 1 + \beta_2 P_2(\cos\theta) + \beta_4 P_4(\cos\theta) + \beta_6 P_6(\cos\theta), \quad (1)$$

where θ is the angle between the photofragment recoil velocity and the laser polarization direction, and the β_k are the kth-order spatial anisotropy parameters. The molecular-frame photofragment alignment can be completely described by an expansion of alignment parameters $\boldsymbol{a}_q^{(k)}(p)$ [2], for which $k \leq 2J$. Additionally, the detection process is sensitive to the $\boldsymbol{a}_q^{(k)}(p)$ with $k \leq 2n$, where n is the number of photons in the resonant step of the $(n + m)$ REMPI process. For this experiment, both J and n are equal to 2 (thus $k \leq 4$), so the complete set of alignment parameters can be measured. It has been shown that the laboratory-frame Legendre coefficients β_k can be expressed in terms of the $\boldsymbol{a}_q^{(k)}(p)$ for $k \leq 4$ [14]:

$$\beta_2 N = c\beta + s_2\left\{A_0^2(\text{sio}) + \frac{1}{7}[2A_0^2(\text{aniso}) + cA_1^2 - 2cA_2^2]\right\} + s_4\left\{\frac{1}{21}[6A_0^4(\text{aniso}) + \sqrt{30}\,cA_1^4 + \sqrt{15}\,cA_2^4]\right\}, \quad (2a)$$

$$\beta_4 N = s_2\left\{\frac{1}{35}[18A_0^2(\text{aniso}) - 12cA_1^2 + 3cA_2^2]\right\} + s_4\left\{A_0^4(\text{iso}) + \frac{1}{77}[20A_0^4(\text{aniso}) + \sqrt{30}\,cA_1^4 - 6\sqrt{15}\,cA_2^4]\right\}, \quad (2b)$$

$$\beta_6 N = s_4\left\{\frac{1}{33}[15A_0^4(\text{aniso}) - 2\sqrt{30}\,cA_1^4 + \sqrt{15}\,cA_2^4]\right\}, \quad (2c)$$

where N (which is proportional to the population) is given by

$$N = 1 + s_2\{\tfrac{1}{5}[A_0^2(\text{aniso}) + cA_1^2 + cA_2^2]\}, \quad (2d)$$

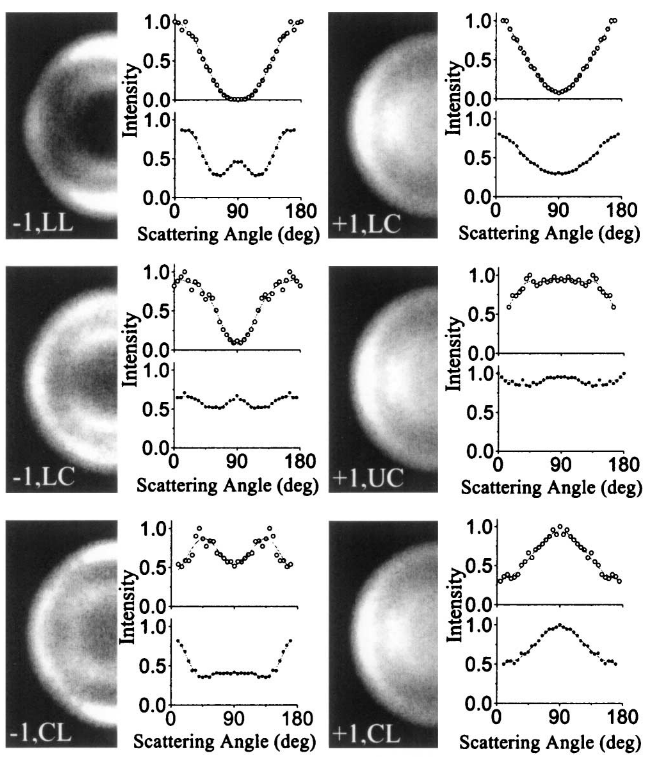

FIG. 1. Six data images of the $S(^1D_2)$ photofragments following the photolysis of OCS at 223 nm. Both the photolysis and probe laser polarizations are vertical. Each image is labeled with the (ΔJ, photolysis polarization, probe polarization) notation. ΔJ refers to the difference in J between the ground and the excited states in the REMPI scheme; L, C, and U denote linear, circular, and unpolarized laser polarizations, respectively. For each image, the angular distributions are shown for the slow channel (open circles) and the fast channel (solid circles).

and the $A_q^k(p)$ [defined to simplify Eqs. (2a)–(2d); the labels (iso) and (aniso) signify the isotropic and anisotropic dependence on the photolysis polarization] are expressed in terms of the $\boldsymbol{a}_q^{(k)}(p)$ and the spatial anisotropy parameter β by

$$\boldsymbol{a}_0^{(k)}(\|) = \frac{1}{(1 + \beta)}[A_0^k(\text{iso}) + A_0^k(\text{aniso})], \quad (3a)$$

$$\boldsymbol{a}_0^{(k)}(\perp) = \frac{1}{(1 - \beta/2)}\left[A_0^k(\text{iso}) - \frac{1}{2}A_0^k(\text{aniso})\right], \quad (3b)$$

$$\text{Re}[\boldsymbol{a}_1^{(k)}(\|, \perp)] = \sqrt{\frac{3}{8}}\,A_1^k, \quad (3c)$$

$$\boldsymbol{a}_2^{(k)}(\perp) = \frac{1}{(1 - \beta/2)}\sqrt{\frac{3}{32}}\,A_2^k, \quad (3d)$$

The factors s_k in Eqs. (2a)–(2d) are the detection sensitivities to the $\boldsymbol{a}_q^{(k)}(p)$. For the $^1F_3 \longleftarrow\!\longleftarrow {}^1D_2$ transition, s_2 and s_4 are equal to $(-1)^\varepsilon(40/49)$ and $(1/6^\varepsilon)(-36/49)$, respectively, and, for the $^1P_1 \longleftarrow\!\longleftarrow {}^1D_2$ transitions, s_2 and s_4 are equal to $(-1)^\varepsilon(5/7)$ and $(1/6^\varepsilon)(-48/7)$, respectively (explicit formulas for the s_k are given in [14], general for all atoms and molecules for 2 + 1 REMPI). The value of ε is 0 and 1 for linearly and circularly polarized (or unpolarized) *probe* light, respectively. The factor c is equal to 1 and $-1/2$ for linearly and circularly polarized (or unpolarized) *photolysis* light, respectively. Notice that β and each $A_q^k(p)$ with $q \neq 0$ are multiplied by the factor c.

A single Abel-invertible image provides three equations [Eqs. (2a)–(2c)] with nine unknowns [β, the four $A_q^2(p)$, and the four $A_q^4(p)$]. Additional orthogonal equations can be generated from images using different detection transitions [which alters the values of the s_k] and different

TABLE I. Speed-dependent anisotropy parameters ($\sigma = 0.1$).

	Slow channel			Fast channel		
$(\Delta J, \varepsilon_{\text{phot}}, \varepsilon_{\text{probe}})$	β_2	β_4	β_6	β_2	β_4	β_6
$(-1, \text{LL})$	2.1	0.2	−0.1	0.7	0.6	−0.4
$(-1, \text{LC})$	1.2	−0.4	0.0	0.0	0.2	0.0
$(-1, \text{CL})$	0.0	−0.5	0.0	0.3	0.5	0.3
$(+1, \text{LC})$	1.6	0.2	0.0	0.7	0.1	0.0
$(+1, \text{CL})$	−0.7	0.1	0.0	−0.5	0.1	0.0
$(+1, \text{UC})$	−0.2	−0.1	0.0	0.1	0.1	0.0

combinations of linearly and circularly polarized probe and photolysis light [which alter the values of c and the s_k]. A minimum of four such images are needed to determine all nine parameters [14].

Abel inversion of the images in Fig. 1 gives the angular distributions shown in Fig. 1, and fitting with Eq. (1) for both the slow and fast velocity channels yields the speed-dependent anisotropy parameters shown in Table I.

For each channel, nonzero values of β_6 (within experimental error) are expected for only two of the six images [$(-1, \text{LL})$ and $(-1, \text{CL})$] for which the factor s_4 is large. Therefore, Table I yields fourteen equations for each channel [using Eqs. (2a)–(2c)]. These equations are grouped into sets of nine orthogonal simultaneous equations, solved numerically, and, using Eqs. (3a)–(3d), the $a_q^{(k)}(p)$ are calculated and plotted in Fig. 3 (below). The error bars are 1σ confidence intervals from the different sets of equations.

The spatial anisotropy parameter, β, is measured to be 0.2 ± 0.1 for the fast channel, and 1.4 ± 0.2 for the slower channel, in approximate agreement with similar measurements for this system [15–17]. The conclusion is supported that the slower channel is produced mostly by the parallel excitation to the A' component of a $^1\Delta$ state, whereas the faster channel is produced by approximately equal excitation to both the $A'(^1\Delta)$ state (via a parallel transition) and the $A''(^1\Sigma^-)$ state (via a perpendicular transition). However, previous analyses of $S(^1D)$ alignment [15,17] did not include noncylindrically symmetric contributions ($q \neq 0$), and detection schemes strongly sensitive to the $k = 4$ parameters were not used. Consequently, quantitative comparison with the present work is not possible; however, there is no qualitative disagreement.

The $a_q^{(k)}(p)$ formalism completely describes the dissociation-angle-dependent photofragment alignment, and further decomposes the photofragment polarization into the incoherent [$a_0^{(k)}(\|)$ and $a_q^{(k)}(\perp)$] and coherent contributions $a_1^{(k)}(\|, \perp)$ from dissociating states accessed by parallel ($\|$) and perpendicular ($\perp$) transitions, in the axial recoil limit [1,2]. In other limits (such as nonaxial recoil and with bent transitions), the interpretation of the parameters changes, but the alignment can still be measured [since the $a_q^{(k)}(p)$ expansion forms a complete basis set]. As shown in Fig. 2,

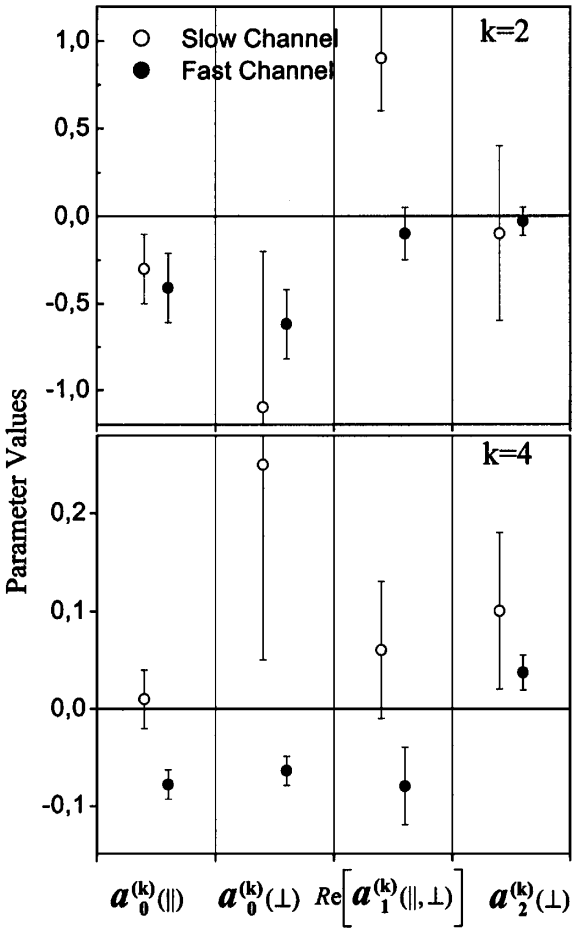

FIG. 2. Complete measurement of the $S(^1D_2)$ photofragment alignment inverted from the data in Table I using Eqs. (2) and (3). For $J = 2$, physical ranges are given by $-1 \leq a_0^{(2)} \leq 1$ and $-1/6 \leq a_0^{(4)} \leq 1/4$.

the $\mathrm{Re}[a_1^{(2)}(\|, \perp)]$ is large (near maximal) for the slow channel but approximately zero for the fast channel. In contrast, Kim *et al.* [16] followed by Rakitzis *et al.* [18]

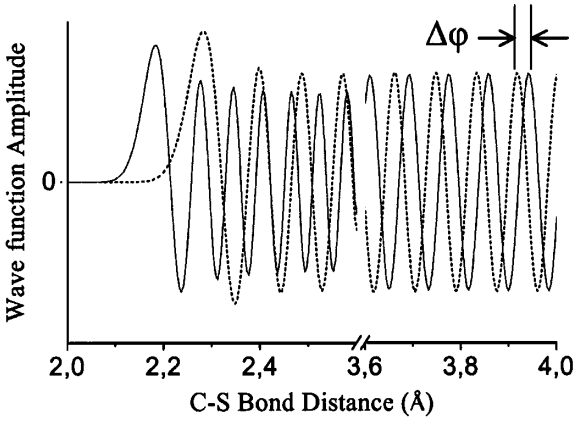

FIG. 3. Wave functions of two dissociative states, showing that the asymptotic phase difference $\Delta\varphi$ of the S-atom wave functions arises from different behavior at small bond distances, where the two dissociative states differ in energy.

TABLE II. $S(^1D_2)$ recoil-frame m-state distributions.

Population	Slow channel		Fast channel	
$p(J, \lvert m\rvert)$	($\parallel$) excitation	($\perp$) excitation	($\parallel$) excitation	($\perp$) excitation
$p(2,0)$	0.31 ± 0.08	1.0 ± 0.5	0.16 ± 0.07	0.24 ± 0.07
$p(2,1)$	0.46 ± 0.10	0.0 ± 0.6	0.73 ± 0.07	0.75 ± 0.07
$p(2,2)$	0.23 ± 0.12	0.0 ± 0.3	0.11 ± 0.11	0.01 ± 0.11

have measured the opposite trend for the $\mathrm{Im}[\boldsymbol{a}_1^{(1)}(\parallel, \perp)]$ parameter: This orientation parameter is large for the fast channel, and approximately zero for the slow channel. In the limit of pure parallel and perpendicular excitations (in the axial recoil approximation), the $q = 1$ parameters can arise only from the interference of the resulting dissociative channels [1,2]. In this limit, the $\mathrm{Re}[\boldsymbol{a}_1^{(k)}(\parallel, \perp)]$ alignment parameters are proportional to $\cos(\Delta\varphi)$, and the $\mathrm{Im}[\boldsymbol{a}_1^{(k)}(\parallel, \perp)]$ orientation parameters are proportional to $\sin(\Delta\varphi)$, where $\Delta\varphi$ is the phase difference between the interfering asymptotic wave functions. Therefore, the observed values of the interference terms can be explained by values for $\Delta\varphi$ of approximately $\pi/2$ and 0 ($\pm n\pi$) for the faster and slower channels, respectively. The phase shift arises from the energy differences between the A' and A'' states during dissociation (see Fig. 3).

The complete photofragment density matrix, and the m-state distributions arising from the parallel and perpendicular excitations for the faster and slower channels, can be calculated directly from the $\boldsymbol{a}_q^{(k)}(p)$ [2], and the latter are tabulated in Table II. In the axial recoil approximation and for linear OCS dissociation, the $A'(^1\Delta)$ state (accessed via a parallel transition, so that the projection of the photon angular momentum along the recoil direction $m_p = 0$) correlates to $S(^1D_2)$ atoms with $m = 0$, whereas the $A''(^1\Sigma^-)$ state (accessed via a perpendicular transition, for which $m_p = \pm 1$) correlates to atoms with $m = \pm 1$ [by conserving the projection of electronic angular momentum; note that $CO(^1\Sigma^+)$ fragments possess $\Omega = 0$]. As expected from this approximation, the population of the $m = 2$ states is small for all observed channels, and the fast channel produced from perpendicular excitation produces mostly $m = \pm 1$ atoms. In contrast, both ($\parallel$)-excitation channels produce significant $m = \pm 1$ populations, indicating nonadiabatic interactions between the A' and the A'' state during the dissociation process [7]. The slight OCS bend angle of about 15° [17] does not affect these arguments significantly.

This work is conducted at the Ultraviolet Laser Facility operating at FORTH-IESL (Improving Human Potential-Transnational Access to Major Research Infrastructures, HPRI-CT-1999-00074) and is also supported by TMR Network *IMAGINE* ERB 4061 PL 97-0264.

*Email address: ptr@iesl.forth.gr

[1] L. D. A. Siebbeles, M. Glass-Maujean, O. S. Vasyutinskii, J. A. Beswick, and O. Roncero, J. Chem. Phys. **100**, 3610 (1994).
[2] T. P. Rakitzis and R. N. Zare, J. Chem. Phys. **110**, 3341 (1999).
[3] A. S. Bracker, E. R. Wouters, A. G. Suits, Y. T. Lee, and O. S. Vasyutinskii, Phys. Rev. Lett. **80**, 1626 (1998).
[4] T. P. Rakitzis, S. A. Kandel, A. J. Alexander, Z. H. Kim, and R. N. Zare, J. Chem. Phys. **110**, 3351 (1999).
[5] T. Peter Rakitzis, S. Alex Kandel, Andrew J. Alexander, Zee Hwan Kim, and Richard N. Zare, Science **281**, 1346 (1998).
[6] Z. H. Kim, A. J. Alexander, S. A. Kandel, T. P. Rakitzis, and R. N. Zare, *Stereochemistry and Control in Molecular Reaction Dynamics* (Faraday Division, Chemical Society, London, 1999), Discussion 113.
[7] A. S. Bracker, E. R. Wouters, A. G. Suits, and O. S. Vasyutinskii, J. Chem. Phys. **110**, 6749 (1999).
[8] A. J. Alexander, Z. H. Kim, S. Alex Kandel, R. N. Zare, T. P. Rakitzis, Y. Asano, and S. Yabushita, J. Chem. Phys. **113**, 9022 (2000).
[9] D. W. Chandler and P. L. Houston, J. Chem. Phys. **87**, 1445 (1987).
[10] A. T. J. B. Eppink and D. H. Parker, Rev. Sci. Instrum. **68**, 3477 (1997).
[11] Z. H. Kim (private communication).
[12] N. Sivakumar, G. E. Hall, P. L. Houston, J. W. Hepburn, and I. Burak, J. Chem. Phys. **88**, 3692 (1988).
[13] Y. Sato, Y. Matsumi, M. Kawasaki, K. Tsukiyama, and R. Bersohn, J. Phys. Chem. **99**, 16 307 (1995).
[14] T. P. Rakitzis, Chem. Phys. Lett. **342**, 121 (2001).
[15] Y. Mo, H. Katayanagi, M. C. Heaven, and T. Suzuki, Phys. Rev. Lett. **77**, 830 (1996).
[16] Z. H. Kim, A. J. Alexander, and R. N. Zare, J. Phys. Chem. A **103**, 10 144 (1999).
[17] T. Suzuki, H. Katayanagi, S. Nanbu, and M. Aoyagi, J. Chem. Phys. **109**, 5778 (1998).
[18] T. P. Rakitzis, P. C. Samartzis, and T. N. Kitsopoulos, J. Chem. Phys. **111**, 10 415 (1999).